

Parametrization of a reactive force field for aluminum hydride

J. G. O. Ojwang,^{1,2,a)} Rutger A. van Santen,¹ Gert Jan Kramer,¹ Adri C. T. van Duin,³ and William A. Goddard III⁴

¹Schuit Institute of Catalysis, Eindhoven University of Technology, Postbus 513, Den Dolech 2, Eindhoven 5600 MB, The Netherlands

²Geophysical Laboratory, Carnegie Institution of Washington, 5251 Broad Branch Rd. NW, Washington D.C. 20012, USA

³Department of Mechanical and Nuclear Engineering, Pennsylvania State University, University Park, Pennsylvania 16802, USA

⁴Materials and Process Simulation Center (MSC), California Institute of Technology, 1200 East California Boulevard, Pasadena, California 91125, USA

(Received 2 April 2009; accepted 26 June 2009; published online 22 July 2009)

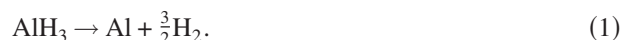
A reactive force field, REAXFF, for aluminum hydride has been developed based on density functional theory (DFT) derived data. REAXFFAlH₃ is used to study the dynamics governing hydrogen desorption in AlH₃. During the abstraction process of surface molecular hydrogen charge transfer is found to be well described by REAXFFAlH₃. Results on heat of desorption versus cluster size show that there is a strong dependence of the heat of desorption on the particle size, which implies that nanostructuring enhances desorption process. In the gas phase, it was observed that small alane clusters agglomerated into a bigger cluster. After agglomeration molecular hydrogen was desorbed from the structure. This thermodynamically driven spontaneous agglomeration followed by desorption of molecular hydrogen provides a mechanism on how mobile alane clusters can facilitate the mass transport of aluminum atoms during the thermal decomposition of NaAlH₄. © 2009 American Institute of Physics. [DOI: 10.1063/1.3182853]

I. INTRODUCTION

One of the major challenges in the quest for hydrogen storage solutions is the development of solid-state hydrogen storage media for vehicles. The United States' Department of Energy (DoE) has set a minimum target of 6 wt % H₂ for economically practical storage of hydrogen in a solid-state material by the year 2010. AlH₃, which has about 10.1 wt % of H₂ and a volumetric density of 0.148 kg H₂/l, is quite attractive as a potential candidate for onboard hydrogen storage applications in proton exchange membrane fuel cells. AlH₃ is a covalently bonded metastable binary hydride, with polymeric (AlH₃)_n forms. There are at least seven (α , α' , β , γ , δ , ϵ , and ζ) known nonsolvated phases of AlH₃.^{1,2} Experimentally, under ambient conditions, the most stable phase of AlH₃ is α -AlH₃, which has a trigonal/rhombohedral crystal structure (space group $R\bar{3}c$) with lattice parameters a = 4.449 Å and c = 11.804 Å.³ The basic building unit of all the AlH₃ polymorphs is the AlH₆ octahedra and the α -AlH₃ polymorphic modification is the most densely packed. In 2005, Ke *et al.*,⁴ using density functional theory (DFT), identified two structures of AlH₃ (cubic $Fd\bar{3}m$ and orthorhombic $Cmcm$), which were theoretically calculated to be more stable than α -AlH₃. In 2006, the Institute for Energy Technology (IFE) experimentally solved the structure of orthorhombic α' -AlH₃. In the same year, a joint collaboration of University of Hawaii (UH), IFE, and Brookhaven National Laboratory (BNL) synthesized and solved the structures of

cubic $Fd\bar{3}m$ (β -AlH₃) and tetragonal $Pnnm$ (γ -AlH₃) using organometallic methods.⁵ All the three structures were found to be less stable than α -AlH₃ at temperatures over 300 K.

The metastable AlH₃ does not release hydrogen under ambient conditions of temperature and pressure. Although all the known AlH₃ phases are thermodynamically unstable with an equilibrium decomposition pressure in the range of kilobars at room temperature, they are usually metastable and slowly decompose at room temperature. The cause of this metastability is the encapsulation of the hydrogen in AlH₃ by a layer of Al₂O₃ that surrounds the surface of the AlH₃ particles. At atmospheric pressure and in the temperature range of 330–400 K, subject to its preparation history, the decomposition of AlH₃ occurs in a single step as follows:



Thermodynamically, this reaction is not easily reversible. To rehydride Al back to AlH₃ hydrogen gas pressures of over 2.5 GPa are needed.^{6,7} AlH₃ has a low decomposition enthalpy of about 1.82 kcal/mol H₂,⁸ which is 20% that of NaAlH₄.⁹ The decomposition rate of AlH₃ can be tuned through nanostructuring (particle size reduction).⁵ However, the decomposition reaction of AlH₃ is not reversible and therefore the desorbed hydrogen must be regenerated off-board. There are various ongoing research efforts to improve the sorption kinetics of AlH₃. Sandrock *et al.* have shown that doping of AlH₃ with small amounts of alkali metal hydrides (LiH, NaH, and KH) leads to accelerated H₂ desorption rates at low temperatures.^{10,11}

^{a)}Electronic mail: ojgojwang@yahoo.com.

TABLE I. Bond energy and bond-order parameters. D_e^σ is in kcal/mol.

Bond	D_e^σ	$P_{be,1}$	$P_{be,2}$	$P_{b0,1}$	$P_{b0,2}$
Al–H	93.4	−0.6599	8.7138	−0.08	6.978

In this work we have parametrized a reactive force field (REAXFFAlH₃) for AlH₃ with the objective of describing the H₂ desorption process in AlH₃. REAXFF has already been shown to be able to accurately predict the dynamical and reactive processes in hydrocarbons,¹² silicon/silicon oxides,¹³ aluminum/aluminum oxides,^{14,15} nitramines,¹⁶ sodium hydride,¹⁷ and magnesium hydride.¹⁸ Herein, the details of the parametrizations of REAXFFAlH₃, the diffusion mechanism of hydrogen atoms and hydrogen molecules in AlH₃, the abstraction process of surface molecular H₂ in AlH₃ cluster, the possibility of phase transition between different polymorphic modifications during the heating process, and the role of alane clusters in the transportation of Al atoms are examined. In addition, interestingly, this paper shows that small alane molecules have to first of all agglomerate before desorption of molecular hydrogen can occur. This is very important in understanding the mass transport of aluminum atoms during the thermal decomposition process of NaAlH₄.^{19–21}

This paper is organized as follows. Section II deals with force field parametrizations and the tests taken to ensure that the force field is well parametrized, Sec. III deals with the dynamics of hydrogen desorption in aluminum hydride clusters and the behavior of alanes on Al(111) surface, Sec. IV focuses on the abstraction process of molecular hydrogen from a cluster of AlH₃, and Sec. V is devoted to the issue of trapped molecular hydrogen in the channels of a cluster of AlH₃. We conclude in Sec. VI.

II. FORCE FIELD PARAMETRIZATIONS

REAXFFAlH₃ has been parametrized in the same way as REAXFF_{NaH} (Ref. 17) and REAXFF_{MgH}.¹⁸ The force field does not use fixed connectivity assignment between atoms but rather the bond-order formalism, which allows for bonds to be created and broken-up in line with the works of Tersoff²² and Brenner.²³ REAXFF calculates nonbonded (van der Waals and Coulomb) interactions between all atoms (including 1–2, 1–3, and 1–4 interactions) making it suitable for systems which have polar-covalent interactions. Implemented in REAXFF are polarizable charges that are calculated using electronegativity equalization method²⁴ (EEM) and which provides a geometry dependent charge distribution.

The fitting data used in REAXFF were obtained from DFT using the efficient and accurate total-energy package, VASP (Vienna *ab initio* simulation package).²⁵ VASP implements a projector augmented plane-wave (PAW) approach.²⁶ In deter-

mining the relaxed geometries of the structures considered in this work, a plane-wave cutoff of 600 eV (1 eV = 23.06 kcal/mol) was used. A convergence of 10^{−6} eV/atom was placed as a criterion on the self-consistent convergence of the total energy. The ions involved are steadily relaxed toward equilibrium until the Hellman–Feynman forces are minimized to less than 0.02 eV/Å using conjugate gradient algorithm during all relaxation runs. A further local optimization was done on the already relaxed structure using quasi-Newton algorithm until the Hellman–Feynman forces on the ions were less than 0.005 eV/Å. To represent electronic-correlation effects for a particular ionic configuration, the calculations used the generalized gradient approximation of Perdew and Wang (GGA-PW91).^{27–29} For cluster calculations, a cubic supercell of side of 20 Å was used and the Brillouin zone was sampled at the Γ point. For all the AlH₃ condensed phases, Brillouin zone integrations were performed using 4 × 4 × 4 *k*-points as per the Monkhorst–Pack grid scheme.³⁰ The reference configurations for valence electrons used were Al(3s²3p¹) and H(1s¹).

To parametrize REAXFF energy expressions, a fitting was done to a training set containing the DFT derived equations of state (EoSs) of pure Al and AlH₃ condensed phases, reaction energies, and bond dissociation profiles on small finite clusters. The bond and atom parameters for REAXFF energy functions (Tables I and II) were determined from Al–Al and Al–H bonds in small AlH₃ clusters such as AlH₃, Al₂H₆, Al₃H₉, Al₄H₁₂, Al₅H₁₅, Al₆H₁₈, Al₇H₂₁, and Al₈H₂₄ and from the EoSs and cohesive energies of Al-metal and AlH₃ condensed phases. The symbols of the parameters in Tables I–IV are shown in Refs. 13 and 16.

Table III shows the EEM parameters (EEM hardness η , EEM electronegativity χ , and EEM-shielding parameter γ). These parameters were optimized to fit Mulliken charge distributions of small representative structures (AlH₃, Al₂H₆, Al₃H₉, and Al₄H₁₂) obtained from DFT calculations. REAXFF successfully reproduces charge transfer for all the clusters considered. The partial charges fitted into the training set were obtained by performing a Mulliken charge distribution analysis in an all electron calculation in CRYSTAL06.^{31,32} CRYSTAL06 implements a localized basis set approach. The radical factors in the all electron basis set are expressed as a linear combination of Gaussian-type functions of the electron-nucleus distance according to 85(*s*)11(*sp*)*G* and 5(*s*)11(*sp*)1(*p*)*G* contractions for Al and H, respectively.³²

TABLE II. Atom parameters ($p_{ov/un}$ is in kcal/mol).

Atom	$p_{ov/un}$	λ_{11}	$p_{v,5}$	$p_{v,6}$
Al	−23.18	2.53	8.0	2.5791
H	−15.76	2.15	1.0	2.8793

TABLE III. Coulomb parameters.

Atom	η (kcal/mol)	χ (kcal/mol)	γ (Å)
Al	4.9	1.8921	0.6191
H	6.5	4.1882	0.7358

TABLE IV. Valence angle parameters.

Angle	$\Theta\Theta_{0,0}$	k_a	k_b	$p_{v,1}$	$p_{v,2}$	p_{pen}	$p_{v,4}$
H–Al–Al	66.95	39.1233	0.1935	0	1.0	0	2.99
H–Al–Al	180.00	−26.6261	5.3467	0	1.0	0	1.01
H–Al–H	70.85	3.4517	8.8151	0	3.0	0	2.40
Al–H–Al	0.00 ^a	36.0088	0.0603	0	3.0	0	1.01

^aThe value leads to an equilibrium angle of $180-0=180^\circ$ for the single bond Al–H–Al valence angle.

To ensure high numerical accuracy the truncation tolerance for the numerical evaluation of bielectronic integrals (both the Coulomb and the Hartree–Fock exchange series) were set at 10^{-8} , 10^{-8} , 10^{-8} , and 10^{-16} .³² All the units are in a.u. (1 a.u.=627.51 kcal/mol).

Table IV shows the optimized valence angle parameters for H–Al–Al and H–Al–H angles. To obtain these quantities, the clusters are first fully optimized in DFT calculations. This is followed by doing single point calculations in which the valence angles are modified while other parameters are fixed. The first line reflects a normal H–Al–Al angle interaction, with an equilibrium angle of 113.05° and force constants of 39.1233 and 0.1935 kcal. The valence angle with a negative force constant (H–Al–Al), -26.6261 kcal, aims to destabilize the case where the hydrogen atom is exactly in between the Al atoms (i.e., H–Al–Al angle is zero degrees). This is effectively an inverted angle function, with a maximum at H–Al–Al equals zero degrees and falling off to zero for different values of this angle.

A. Bond dissociation, angle bending, and binding energies

Figure 1(a) shows the bond dissociation curve of AlH_3 , while Fig. 1(b) shows the angle bending-energy curve of the AlH_3 molecule used to optimize the valence angle parameter of REAXFF/ AlH_3 . These DFT curves were used to optimize the bond energy in the reactive potential. The dissociation curves were constructed from the equilibrium geometry using single point calculations by changing the bond length. REAXFF gives an equilibrium bond length of 1.6 \AA , which is in excellent agreement with DFT value of 1.59 \AA . The energies were computed with reference to the equilibrium bond length's energy. To optimize the valence angle parameter the geometry of the AlH_3 molecule was minimized for various fixed values, viz 120° , 115° , 110° , ..., 65° , 60° . REAXFF predicts that the H–Al–H equilibrium angle is 120° . This is in excellent agreement with DFT. For smaller angles, DFT

gives larger energy barriers than REAXFF due to electron-electron repulsion inherent in the former. For instance, at 60° the AlH_3 is destabilized by 44.4 kcal/mol in DFT, whereas REAXFF, which does not care about electrons, gives a destabilization energy of 11.66 kcal/mol .

Table V shows the DFT values versus REAXFF values of adsorption energies of hydrogen on Al(111) surface. The adsorption energy E_{ads} is defined as $E_{\text{ads}}=[E_{(\text{S/H})}-E_{\text{S}}-nE_{(\text{H})}]/n$, where $E_{(\text{S/H})}$ is the total energy of hydrogen-adsorbed aluminum slab, E_{S} is the total energy of aluminum slab, E_{H} is the total energy of hydrogen atom (-25.79 kcal/mol), and n stands for the number of adsorbed hydrogen atoms. In the context of this definition, $E_{\text{ads}} < 0$ corresponds to exothermic adsorption. To calculate E_{H} , two hydrogen atoms were placed 12 \AA apart in a cubic box of side of 20 \AA . The Brillouin zone was sampled at the gamma point. The total energy of the hydrogen atom was then taken as half the calculated total energy. The Al surface was modeled by a repeated slab of five layers, giving a slab thickness of 9.6 \AA . A vacuum equivalent to a slab with five layers of aluminum atoms was imposed in the z -direction to separate the slab from its periodic images. H is adsorbed on one side of the slab only. The top two layers plus the H atom are relaxed while the bottom three layers are fixed at their bulk positions. The Brillouin zone was sampled using a well converged $9 \times 9 \times 1$ k -points.

REAXFF gives decent adsorption energies in comparison to DFT predictions (Table V). From DFT calculations, atomic hydrogen preferably adsorbs on the fcc site. This is consistent with the work of Stumpf,³³ who showed that H preferably adsorbs on the fcc site with an exothermic adsorption energy from -45.58 to -45.89 kcal/mol (depending on the coverage). This value can be slightly higher or lower depending on the exchange-correlation functional (LDA, PBE, or PW91) used. In agreement with Stumpf, we calculated the fcc adsorption energy to be -47.63 kcal/mol . From REAXFF, the adsorption energies for bridge, hcp, and top sites

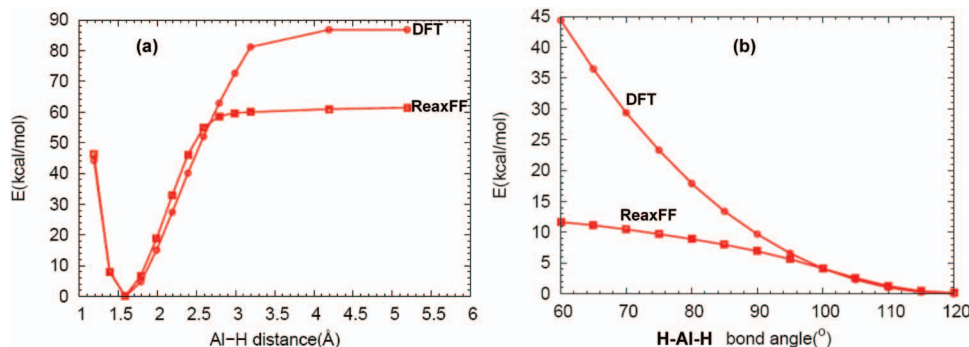


FIG. 1. (a) Bond dissociation profile of AlH_3 . REAXFF gives an equilibrium bond length of 1.6 \AA . This is in excellent agreement with DFT value of 1.59 \AA . (b) H–Al–H angle bend in AlH_3 molecule. The energies are computed with reference to the equilibrium angle energy.

TABLE V. Adsorption energies of hydrogen atoms on the high symmetry sites on Al(111) surface. The energies are in kcal/mol per H.

Site	DFT	REAXFF
hcp	−44.80	−47.80
fcc	−47.63	−49.24
Top	−45.87	−47.14
Bridge	−47.37	−48.93

are −47.37, −44.80, and −45.87 kcal/mol, respectively.

For Al(111) hcp site DFT gives a value of −44.8 kcal/mol per H, while REAXFF gives −47.8 kcal/mol. For Al(111) fcc site DFT predicts the adsorption energy to be −47.63 kcal/mol, while REAXFF gives −49.24 kcal/mol. For the Al(111) top site REAXFF predicts the adsorption energy to be −47.14 kcal/mol, which is in good agreement with the DFT value of −45.87 kcal/mol. The DFT calculated energy barrier for H hopping from the bridge to the fcc site is 2.07 kcal/mol. REAXFF gives a migration energy barrier of 2.7 kcal/mol, which is in excellent agreement with the DFT value. These values are in good agreement with those of Hjelmberg who determined the diffusion energy barrier of H from the bridge to threefold site to be in the range of 2.3–4.6 kcal/mol.³⁴

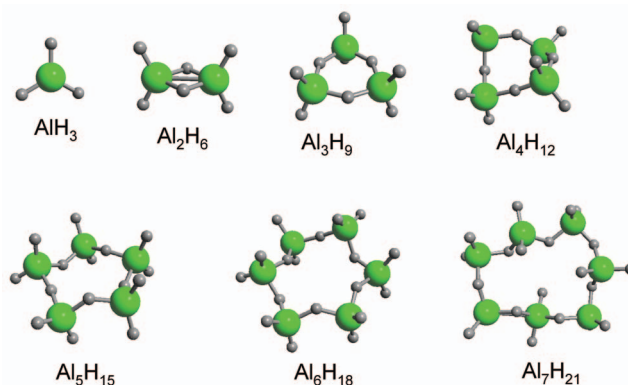
Since the goal of this force field was to study the interaction of alane clusters in the gas phase and on aluminum surface, we also considered the binding energies of alane molecules on Al(111) surface. These energies for various alane cluster models are tabulated in Table VI. As can be seen in Table VI REAXFF gives values that are quite close to DFT values.

That said, there is an increasing interest in studying small clusters of aluminum hydride since nanostructuring might be the key to hydrogen storage in AlH_3 system. During the thermal decomposition process of large systems of aluminum hydride, it is possible that the release of hydrogen and subsequent formation of aluminum clusters occurs in tandem with cluster fragmentation.¹⁷ Herein, we make a comparison between DFT's binding energies and REAXFF binding energies for AlH_3 , Al_2H_6 , Al_3H_9 , Al_4H_{12} , and Al_5H_{15} clusters. These small clusters are shown in Fig. 2.

Kawamura *et al.*³⁵ have given an extensive study of small AlH_3 clusters and have shown that the energetics are very close for singly bridged cyclic, doubly bridged cyclic, and linear clusters. In general, the singly bridged structures are more favored over the doubly bridged structures. However, Kawamura *et al.* also found out that in some instances, due to exchange-correlation effects, the doubly bridged structures are preferred to singly bridged structures. In RE-

TABLE VI. Binding energies of AlH_3 , Al_2H_6 , and Al_3H_9 on Al(111) surface.

Cluster	DFT (kcal/mol)	REAXFF (kcal/mol)
AlH_3 on terrace (horizontal)	−20.98	−15.18
Al_2H_6 on terrace	−49.81	46.95
Al_3H_9 on terrace	−51.65	−44.39

FIG. 2. Small representative $[\text{AlH}_3]_n$, $n=1-7$, clusters used in the training set of REAXFF.

AXFF computations, it was seen that for Al_nH_{3n} ($n \geq 4$) the doubly bridged structures are preferred while the singly bridged structures are unstable. This can be understood from the fact that the more the interconnectivity of the Al–H bonds the stronger the bonding. Doubly bridged structures have more bonds and therefore bound to be more stable than singly bridged structures. Table VII shows the binding energies of various $(\text{AlH}_3)_n$ clusters considered in this work. Here, the binding energy is defined as:

$$\text{BE} = -[E(\text{Al}_n\text{H}_{2m}) - E(\text{Al}_{\text{fcc}}) - mE(\text{H}_2)]/m, \quad (2)$$

where $E(P)$ is the total energy of particle P in the ground state. For molecular hydrogen, in DFT, $E_{\text{tot}} = -156.87$ kcal/mol. The total energy of molecular hydrogen was used because in REAXFF the total energy is computed with reference to the isolated atomic species. The DFT values are consistent with the works of Kawamura *et al.* However, Kawamura *et al.* used the total energy of atomic hydrogen instead of that of molecular hydrogen. Therefore, in Table VIII we make a comparison between DFT values and the work of Kawamura *et al.*³⁵ using the total energy of atomic hydrogen, $E_{\text{tot}} = -25.79$ kcal/mol. There is an excellent match between our calculated DFT values and those from the work of Kawamura *et al.*, which was done at the LCAO+GGA level of theory. It can be seen in the table that there is a slow decrease in binding energy per hydrogen of these clusters with increasing cluster size. This is contrary to the expectation that the binding energy per hydrogen should increase concomitantly with increase in cluster size. The decrease in the binding energy can be attributed to the fact that as the cluster size increases so does the free energy of pure aluminum clusters, which raises the cost of fragmenting the

TABLE VII. Binding energies BEs (in kcal/mol H_2) of small AlH_3 clusters used in the training set.

Cluster	DFT	REAXFF
AlH_3	30.77	32.51
Al_2H_6	22.60	28.66
Al_3H_9	29.72	30.13
Al_4H_{12}	39.33	34.50
Al_5H_{15}	42.88	38.80

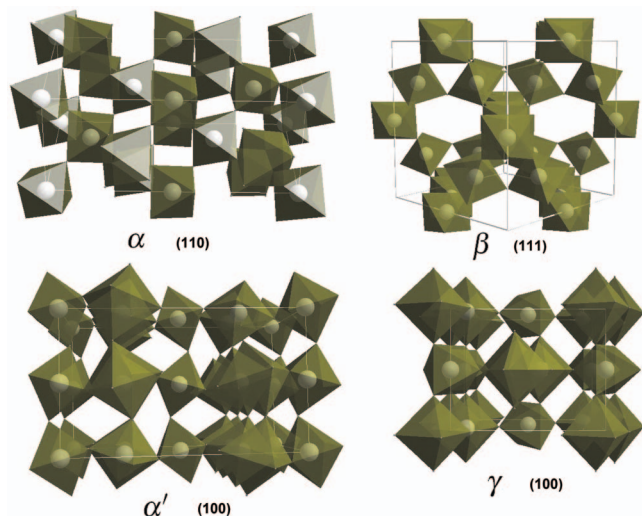
TABLE VIII. Comparison between DFT and binding energies BEs of Kawamura *et al.* (in kcal/mol H) of small AlH_3 clusters.

Cluster	DFT	Ref. 35
AlH_3	68.79	67.50
Al_2H_6	70.01	70.29
Al_3H_9	64.98	65.19
Al_4H_{12}	63.53	62.70
Al_5H_{15}	61.52	60.65
Al_6H_{18}	60.21	59.22
Al_7H_{21}	58.60	57.63
Al_8H_{24}	58.50	58.60

aluminum clusters to accommodate hydrogen atoms.

In the condensed state, for each an every phase of AlH_3 (α , α' , β , and γ) polymorphic modifications considered in this work, the DFT energies were computed for a broad range of volume describing both expansion and compression. Figure 3 shows the crystal structure of the four polymorphs of AlH_3 (α , α' , β , γ) considered in this work. All the AlH_3 polymorphs are made up of three dimensional networks of AlH_6 units. α - AlH_3 crystallizes in the trigonal $R\bar{3}c$ space group, β - AlH_3 crystallizes in the cubic $Fd\bar{3}m$ space group, α' - AlH_3 crystallizes in the $Cmcm$ space group, and γ - AlH_3 crystallizes in the orthorhombic $Pnnm$ space group.

The issue of the relative stability of AlH_3 polymorphic modifications is quite interesting. Experimentally, α - AlH_3 is the most stable polymorph for temperatures greater than or equal to 300 K.³ Theoretically, Ke *et al.*,⁴ using DFT, found β - AlH_3 polymorphic modification of AlH_3 to be the structure with the lowest energy. It is possible that at 0 K the β -phase is indeed more stable than the α -phase as found by Ke *et al.* On the other hand, the relative energy differences between these two phase are in the order of 1 kcal/mol. It might be that it is difficult for DFT to resolve this small energy difference. We found that indeed the cubic β - AlH_3 has the lowest energy. However, this result seems to be an artifact of the pseudopotential (PP) used. For the PAW PPs the β - AlH_3

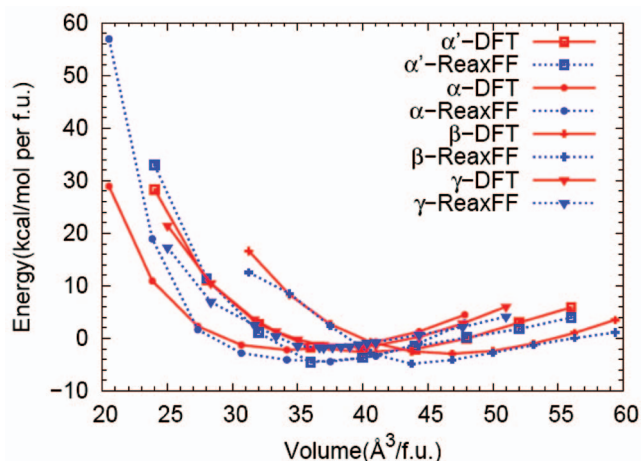
FIG. 3. The various polymorphic modifications of AlH_3 illustrated by the connection of the AlH_6 octahedra and channels through the polymorphs.TABLE IX. Relative stability of three AlH_3 phases with respect to the $R\bar{3}c$ phase using the PAW and US-PP and REAXFF. The units are in kcal/mol.

Phase	PAW	US-PP	REAXFF
$R\bar{3}c$	0	0	0
$Fd\bar{3}m$	-0.76	-0.76	-0.02
$Cmcm$	-0.39	-1.04	+0.38
$Pnnm$	+0.53	+0.51	+2.56

phase has the lowest energy, whereas for ultrasoft (US) PP α' - AlH_3 phase has the lowest energy, see Table IX. In both cases, however, the relative energy differences between α , α' , and β phases are less than 1 kcal/mol. This implies that it should be possible for these phases to transform into one another at certain temperatures and pressures. In particular, since the β phase has more open channels, it can transform to the α phase during the desorption of molecular hydrogen but only if the α phase is more stable. We did not include the ZPE corrections. In the work of Ke *et al.*, zero point energy (ZPE) corrections were included.

Figure 4 shows the EoS for the $R\bar{3}c$ (α - AlH_3), $Fd\bar{3}m$ (β - AlH_3), $Pnnm$ (γ - AlH_3), and $Cmcm$ (α' - AlH_3) phases of AlH_3 . REAXFF correctly describes the EoS of the four phases of AlH_3 and excellently estimates their relative phase stability *vis-à-vis* the DFT's predictions. For instance, DFT (PAW) predicts that β - AlH_3 is more stable than γ - AlH_3 by 0.76 kcal/mol H_2 , whereas REAXFF gives a value of 0.02 kcal/mol H_2 . The experimental heat of formation, for the condensed phase, of AlH_3 range from -2.37 ± 0.1 kcal/mol H_2 (Ref. 2) to -2.72 ± 0.2 kcal/mol H_2 ,⁸ while the calculated values are in the range from -1.66 kcal/mol H_2 (Ref. 36) to -2.95 kcal/mol H_2 .⁴ For α - AlH_3 phase, both DFT and REAXFF give bulk values that are consistent with the calculated values, with DFT giving a value of -2.36 kcal/mol H_2 and REAXFF giving -3.01 kcal/mol H_2 . These values were calculated by comparing to Al(fcc) at its most stable volume and 1.5 H_2 (gas).

During the thermal desorption process there might be phase transformations/crystal modifications or conforma-

FIG. 4. EoSs for AlH_3 phases (DFT values are drawn using straight lines while those for REAXFF are drawn using dotted lines).

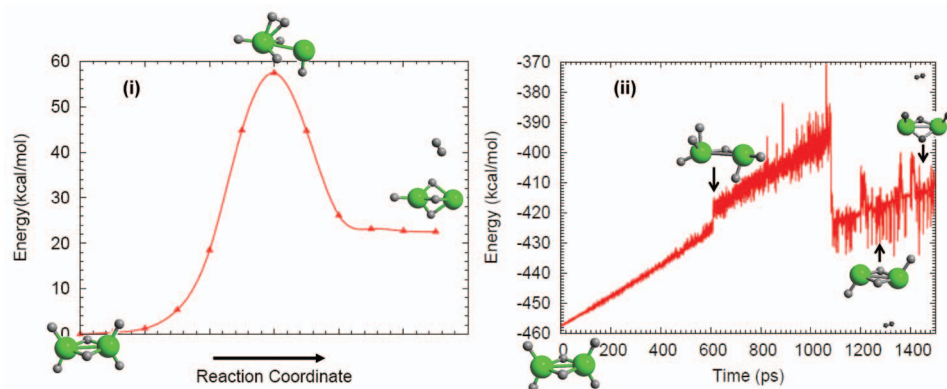


FIG. 5. (i) Dissociation profile of Al₂H₆ as calculated by DFT using nudged elastic band method. (ii) The energy profile during a MD simulation of a heating run of Al₂H₆. The temperature was ramped up at a rate of 0.000 25 K/iteration.

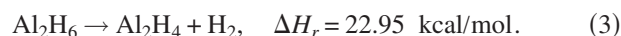
tional changes in both Al and AlH₃ systems. Graetz *et al.*² showed that transitions between α , β , and γ phases are exothermic and likely to occur spontaneously even at room temperature. Further, Grove *et al.*³⁷ showed that in the case of deuterated Al, there is a phase transformation of both β -AlD₃ and γ -AlD₃ to α -AlD₃ starting at 353 and 363 K, respectively. Maehlen *et al.*³⁸ observed a phase transformation of γ -AlH₃ to α -AlH₃ during the decomposition process of the former. There have been claims that such transitions are expected and, in fact, are indicative that the system transforms to a less stable structure. However, it should be noted that the formation of the various polymorphs of AlH₃ depends on their preparation history. Second, a clear sign that the resulting structure is more stable than the starting structure is to do the reverse process, i.e., reduce the temperature to 0 K. If indeed the structure is more stable it should not transform back to the starting (β) phase. It is important to emphasize that the α -AlH₃ is considered stable for temperatures ≥ 300 K. Therefore, it is possible that for temperatures below 300 K the β phase can be more stable than the α phase.

Since REAXFF was parametrized using DFT values, it has that the β phase is the most stable phase. To reflect the experimental observations on relative stabilities of the four aluminum hydride phases (especially the experimentally observed phase transition of β - to α -phase during heating process), we modified the force field so as to make the α -phase the most stable. In the work of Graetz *et al.* the heats of formation of the three polymorphic modifications are as follows: α -AlH₃ (−2.366 kcal/mol H₂), β -AlH₃ (−1.912 kcal/mol H₂), and γ -AlH₃ (−1.617 kcal/mol H₂). We modified REAXFF by these values so as to reflect the experimental results. For the modified force field, the heats of formation of the three polymorphic modifications are as follows: α -AlH₃ (−4.32 kcal/mol H₂), β -AlH₃ (−1.40 kcal/mol H₂), and γ -AlH₃ (−0.17 kcal/mol H₂). These values are in good agreement with the experimental values of Graetz *et al.*²

III. DYNAMICS OF HYDROGEN DESORPTION

An important part of force field parametrization is to get the right reaction dynamics during the thermal decomposition of a cluster (or bulk) of aluminum hydride. Therefore, to ascertain that the force field reproduces the right thermal

decomposition dynamics, we heated up a representative aluminum hydride cluster (Al₂H₆). Al₂H₆ decomposes endothermically as follows:



The transition state and the minimum energy path (MEP) for the process in Eq. (3) was calculated in VASP (DFT) using NEB.³⁹ This is shown in Fig. 5(i). In the NEB simulation it was ascertained that both end points were stable manifolds by performing frequency analysis. To get an accurate identification of the saddle point the climbing image flag was turned on.⁴⁰ This has the effect of driving up to the saddle point the image with the highest energy. This permits an accurate determination of the transition state. To compute the activation energy barrier, the image at the top of the MEP was further locally optimized in VASP using quasi-Newton algorithm. The barrier was calculated to be 51 kcal/mol. In REAXFF the barrier was calculated to be 50 kcal/mol. In general, the dissociation process is endothermic but since the transition state is at a higher energy than the end point, then a fall in potential energy during the stage where molecular hydrogen is released is expected, which indicates that this portion of the reaction is an exothermic process. This is also reflected in Fig. 5(ii), which shows the energy profile during a molecular dynamics (MD) simulation of a heating run of Al₂H₆ at 0.000 25 K/iteration. In the MD simulation, velocity Verlet algorithm was used and the temperature was increased linearly by velocity scaling. The dynamics of hydrogen desorption in the two instances are similar. In Fig. 5(ii) there is a slight rise in energy at about 600 ps. This energy rise occurs due to the distortion of the Al₂H₆ structure. Also shown in Fig. 5(ii), after fragmentation of Al₂H₆ into Al₂H₄ and H₂, are the various geometrical modifications of the resultant Al₂H₄ during the heating process. The most important point to note in Fig. 5(ii) is that like in DFT, the desorption of molecular hydrogen in MD simulation is accompanied by a fall in the potential energy just after the transition state. This gives confidence that the force field reproduces the right desorption dynamics in comparison to DFT.

Table X shows the approximate temperature at which molecular hydrogen was desorbed (cluster dissociation) from various Al_nH_{3n} clusters. These temperatures are an approximation. In reality, the true fragmentation/desorption temperatures might be much lower, subject to long equilibration times, which is beyond the timescale of our simulation. The

TABLE X. The temperature at which molecular hydrogen is released from Al_nH_{3n} cluster. As the size of the cluster increases the temperature at which molecular hydrogen is released from the cluster also decreases.

Cluster	T (K)
AlH_3	2100
Al_2H_6	1900
Al_3H_9	1700
Al_4H_{12}	1400
Al_5H_{15}	1200

most important thing to note here is the decrease in fragmentation/desorption temperature with increase in the size of clusters.

In all the simulation runs, a heating rate of 0.000 25 K/iteration was used because at a heating rate of 0.0025 K/iteration molecular AlH_3 (alane) remained intact throughout the heating range. There are a number of factors that contribute to the temperature at which molecular hydrogen is desorbed from the cluster. First, the length of equilibration. For instance, molecular hydrogen was only desorbed from Al_3H_9 after equilibrating at this temperature (1700 K) for 3500 ps (3.5 ns). When the cluster was heated up from 1 to 2000 K at a rate of 0.000 25 K/iteration, it fragmented into AlH_3 and Al_2H_6 without molecular hydrogen being desorbed. Second, as mentioned in the foregoing, during the heating process these clusters fragment into smaller clusters (which reaggregate) prior to desorption of molecular hydrogen. This fragmentation and reagglomeration process occurs throughout the heating range, once the temperature of the cluster has been elevated (roughly at temperatures greater than 700 K, in the timescale of our simulation). We term this phenomenon as dynamic fragmentation-agglomeration. The reason for fragmentation is that at elevated temperatures the system is already at the threshold where it can fragment into smaller clusters. However, the fragments are less stable. As a result they again agglomerate so as to attain greater stability. The agglomeration process is exothermic and is therefore accompanied by a local rise in temperature. This local rise in temperature facilitates the dissociation of Al–H bonds resulting in the desorption of molecular hydrogen. The calculated energy costs for fragmentation of Al_4H_{12} into smaller clusters are summarized in Table XI. During the heating process Al_4H_{12} fragmented into smaller clusters as follows: First, it fragmented into $\text{Al}_3\text{H}_9 + \text{AlH}_3$. This was then followed by reagglomeration back to Al_4H_{12} . The reagglomerated Al_4H_{12}

TABLE XI. The heat of fragmentation of Al_4H_{12} into various clusters during thermal heating of the cluster. The DFT values were computed using VASP at the PW91 level of theory. The energies are in kcal/mol.

Starting products	DFT(PW91)	REAXFF
$\text{Al}_4\text{H}_{12} \rightarrow \text{Al}_4\text{H}_{10} + \text{H}_2$	20.92	18.77
$\text{Al}_3\text{H}_9 + \text{AlH}_3$	21.16	29.15
$\text{Al}_2\text{H}_6 + \text{Al}_2\text{H}_4 + \text{H}_2$	28.82	32.61
$\text{Al}_2\text{H}_4 + 2\text{AlH}_3 + \text{H}_2$	67.75	66.93

then refragmented into $\text{Al}_3\text{H}_9 + \text{AlH}_3$. This was then followed by reagglomeration and a further fragmentation into Al_2H_6 , Al_2H_4 , and H_2 .

As shown in Table XI, Al_4H_{12} can fragment into Al_3H_9 and AlH_3 at an energy cost of 21.16 kcal/mol (DFT). This is quite close to the dissociation reaction $\text{Al}_4\text{H}_{12} \rightarrow \text{Al}_4\text{H}_{10} + \text{H}_2$, which costs 20.92 kcal/mol. This shows that it is possible that during the heating up process a given cluster of (Al_nH_{3n}) can fragment into smaller clusters prior to desorption of molecular hydrogen once the temperature required to facilitate fragmentation has been reached.

The DFT calculated activation barrier of AlH_3 fragmentation (i.e., $\text{AlH}_3 \rightarrow \text{Al} + \text{H}_2$) in the gas phase is 96.94 kcal/mol and that for Al_2H_6 decomposition (i.e., $\text{Al}_2\text{H}_6 \rightarrow \text{Al}_2\text{H}_4 + \text{H}_2$) is 51 kcal/mol. By comparison the experimental activation energy for hydrogen desorption in $\alpha\text{-AlH}_3$ is 23.22 kcal/mol H_2 .⁴¹ The activation energy barrier for fragmentation of alane is almost four times that for desorption of molecular hydrogen from bulk AlH_3 . This large difference cannot be due to computational inaccuracies. This implies that the fragmentation temperature of alane is much higher than the temperature of desorption of hydrogen from bulk AlH_3 . For instance, in the timescale of our simulation, we find that molecular hydrogen dissociates from Al_2H_6 at about 1900 K. For bulk AlH_3 , in the timescale of our simulation, molecular hydrogen desorbs at 700 K. This is clearly much less than the dissociation temperature of alane. From this comparison, it is clear that alane dissociates at a relatively higher temperature in comparison to bigger clusters. It follows therefore that if alanes were to be the facilitators of mass transport of aluminum atoms during the thermal decomposition of NaAlH_4 (as suggested in Refs. 20 and 21), there must be a different mechanism by which they can release molecular hydrogen at lower temperature. One mechanism is that alanes undergo oligomerization. We discuss this issue in Sec. III A.

A. Gas phase behavior of alanes

Figure 6(a) shows the dimerization of two AlH_3 molecules, while Fig. 6(b) shows the agglomeration of two Al_2H_6 molecules resulting in the formation of a doubly bridged Al_4H_{12} molecule. The NVT (constant number of particles, constant volume, and constant temperature) simulation was done at 300 K using Berendsen thermostat⁴² for 30 ps. The molecules were placed in a cube of side of 20 Å. The dimerization of AlH_3 molecules is in agreement with the well known fact that as the size of AlH_3 clusters increases so does its stability with respect to the individual AlH_3 species. Higher alanes can be easily formed from smaller alanes since the agglomerated alanes are more stable than the individual alane species.³⁵ The theoretical formation energies of Al_2H_6 molecule from two alane molecules as computed by DFT and REAXFF are -19.47 kcal/mol AlH_3 and -18.2 kcal/mol AlH_3 , respectively. The DFT value is consistent with the previous works in Refs. 43–46. From Fig. 6(a), the dimerization energy for alanes is approximately -19 kcal/mol per AlH_3 . This is consistent with the calculated value in Table XII, which shows the energy of agglomeration of various small clusters of Al_nH_{3n} series as calculated using DFT and

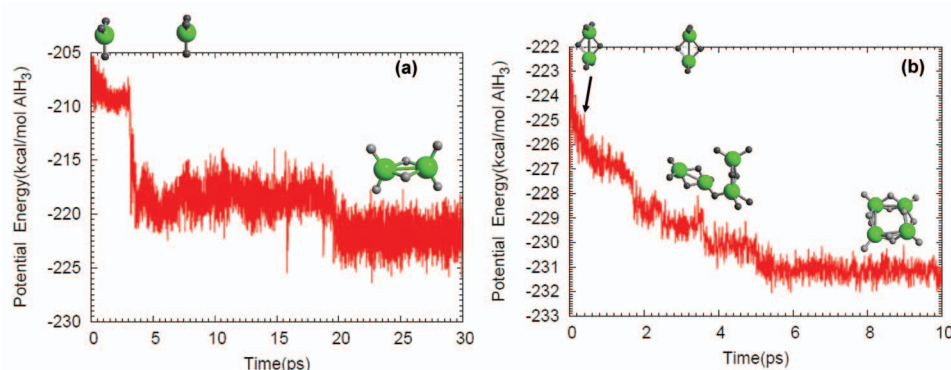


FIG. 6. Illustrations of the atomic configurations and energy profiles for (a) alane dimerization reaction and (b) agglomeration of Al_2H_6 molecules.

REAXFF.

To study the correlation between agglomeration and desorption of molecular hydrogen, we did a MD simulation using 20 Al_2H_6 molecules. We used Al_2H_6 molecules because Al_2H_6 molecule is more stable relative to two alanes (AlH_3 molecules). The molecules were placed at least 10 Å apart in a cubic box of side of 80 Å. The system was first minimized to find the nearest metastable state. After minimization, the system's temperature was ramped up to 1000 K. This was then followed by a *NVT* MD equilibration period, using Berendsen thermostat. The temperature of 1000 K was chosen because we wanted to observe the desorption of molecular hydrogen during the agglomeration process. As will be shown later, even in the temperature range of 300–800 K agglomeration still takes place but molecular hydrogen is not desorbed. In the equilibration process, at 0 ps, the following molecules/clusters exist in the system: Al_8H_{24} , two Al_6H_{18} , two Al_4H_{12} , and six Al_2H_6 . This is so because during the minimization and temperature ramping up process some of the Al_2H_6 molecules agglomerated. As illustrated in Fig. 7, at the end of the simulation there are two molecular hydrogens desorbed from the agglomerated cluster.

A number of factors contribute to desorption of molecular hydrogen. First, the agglomeration process is exothermic. Although, globally, the temperature is kept constant by a thermostat, there is a local rise in temperature due to exothermic nature of the agglomeration process. This local rise in temperature facilitates the instantaneous dissociation of the Al–H bond. Therefore, it becomes easy to desorb molecular hydrogen at this temperature (1000 K). Second, the growth of the cluster leads to the existence of many surface atoms, which are weakly bonded to aluminum atoms. Bigger clusters provide more facile paths for hydrogen desorption as they can make Al–Al metal bonds to compensate for the loss of Al–H bonds. Although the local rise in temperature during

the agglomeration process might play a role in hydrogen desorption, in the long term limit, large cluster size effect is the major contributor to desorption of molecular hydrogen.

In Fig. 7 the snapshot at 0 ps shows the initial clusters after being heated up to 1000 K. Already at this stage some Al_2H_6 molecules have agglomerated. Notice the ringlike conformation of Al_6H_{18} in Fig. 7. At 260.9375 ps the cluster present in the system is $\text{Al}_{40}\text{H}_{120}$, implying that all the small clusters have agglomerated into one cluster. At 261 ps the cluster undergoes partial fragmentation leading to the formation of $\text{Al}_{39}\text{H}_{117}$ and AlH_3 . This partial fragmentation and reagglomeration goes back and forth throughout the simulation period. The first molecular hydrogen is desorbed at 267.875 ps, leading to the formation of the following clusters/molecules: $\text{Al}_{39}\text{H}_{114}$, AlH_4 , and H_2 . Actually, the AlH_4 moiety is quite unstable and is immediately reabsorbed back by the bigger cluster. At 286.25 ps we have the following clusters/molecules: Al_7H_{23} , $\text{Al}_{33}\text{H}_{95}$, and H_2 . At the end of the simulation (1000 ps) the clusters/molecules present in the system are $\text{Al}_{40}\text{H}_{116}$ and two molecular hydrogens. What is quite interesting is that in the end structure (at 1000 ps) there is a central aluminum atom which has six neighboring hydrogen atoms. This is illustrated in Fig. 7(b). The central aluminum atom is in a pentagonal ring of aluminum atoms, which resembles the coordination of aluminum in $\beta\text{-AlH}_3$.

In a different simulation run, in which the temperature of the system was kept fixed at 800 K, the Al_2H_6 molecules agglomerated into $\text{Al}_{40}\text{H}_{120}$ cluster during the 500 ps simulation run. However, at this temperature no molecular hydrogen was desorbed. Further tests (simulations) showed that in the temperature range of 300–800 K the Al_2H_6 clusters agglomerated into one cluster ($\text{Al}_{40}\text{H}_{120}$). However, in these cases no molecular hydrogen was desorbed from the cluster. Figure 8(a) shows the agglomerated structure while the pair distribution function for the annealed (to 0 K) agglomerated cluster is illustrated in Fig. 8(b). The figure shows that the radial distribution function has a slightly broad delta peaks. This suggests that the cluster is in a quasicrystalline state. The quasicrystalline state can be explained by the fact that the aluminum and hydrogen atoms are somehow arranged in a semiperiodic pattern. The average Al–Al distance is approximately 3.0 Å. This value compares quite well to the DFT calculated Al–Al bond length in $\beta\text{-AlH}_3$ (3.2 Å). However, this structure does not have the local coordination of any of the condensed phases of AlH_3 . There are some central

TABLE XII. The energy of agglomeration (per AlH_3) of various small clusters of the Al_nH_{3n} series as calculated using DFT and REAXFF.

Cluster	DFT	REAXFF
$2\text{AlH}_3 \rightarrow \text{Al}_2\text{H}_6$	−19.47	−18.17
$3\text{AlH}_3 \rightarrow \text{Al}_3\text{H}_9$	−20.86	−22.46
$4\text{AlH}_3 \rightarrow \text{Al}_4\text{H}_{12}$	−20.94	−23.88
$5\text{AlH}_3 \rightarrow \text{Al}_5\text{H}_{15}$	−22.19	−24.74
$6\text{AlH}_3 \rightarrow \text{Al}_6\text{H}_{18}$	−20.90	−25.27

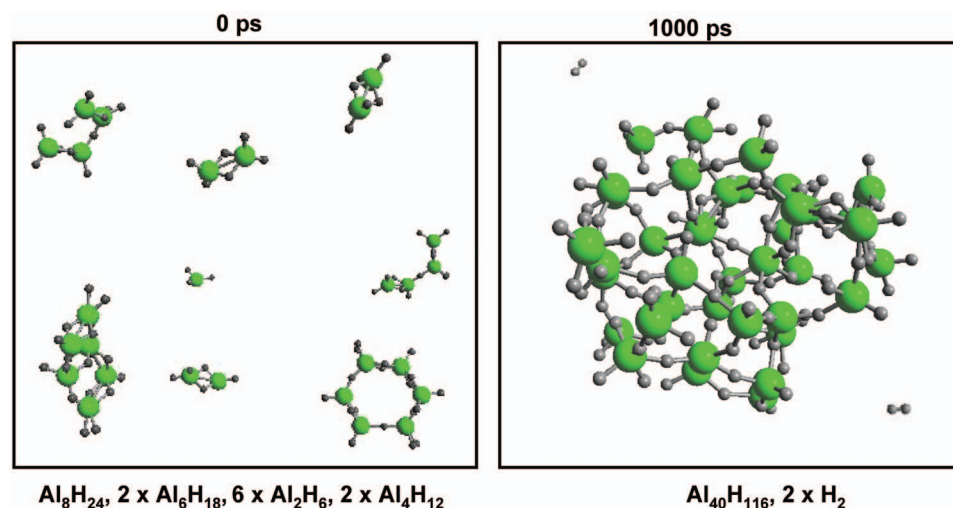


FIG. 7. Snapshots of the Al_2H_6 clusters at the (a) beginning and (b) end of the simulation.

Al atoms that are five coordinated in hydrogen, while the rest have four hydrogen neighbors. The changes in charge redistribution as a result of agglomeration (i.e., plots of the clusters at the beginning of the simulation and that of the agglomerated cluster at the end of the simulation run) are shown in Fig. 9. The figure shows that at the end of the simulation run (500 ps), there is an upward shift on the charge on aluminum atoms as compared to at the beginning of the simulation. Therefore there is a substantial charge transfer from aluminum atoms to hydrogen atoms during the agglomeration process. The distribution of charge on aluminum atoms is also less than the nominal charge of aluminum, implying that the bonding between Al and hydrogen is covalent. Although there is an increase in the negative charge on hydrogen atoms a considerable number still have charges in the range -0.1 to -0.5 . These are the surface hydrogen atoms as can be seen in Fig. 8.

IV. ABSTRACTION OF MOLECULAR HYDROGEN

An important question in hydrogen storage is knowing the nature of structural transformation that takes place during the desorption process of hydrogen. In order to get a better insight of structural transformation during the desorption of hydrogen, we simulated successive abstraction of surface molecular hydrogen from a representative aluminum hydride

nanoparticle ($\text{Al}_{28}\text{H}_{84}$ cluster). This is illustrated in Fig. 10. The abstraction process of surface molecular hydrogen is given by:



where $n=84-0$. The desorption energy is defined as

$$E^{\text{desorb}} = [E_{\text{Al}_{28}\text{H}_{84-n}} + E_{n/2\text{H}_2}] - E_{\text{Al}_{28}\text{H}_{84}}, \quad (5)$$

where $n=2, 4, 6, 8, \dots, 48, 50, 52, \dots, 84$.

Systematically, in the abstraction process, clusters were first minimized and then annealed to 0 K using MD simulation to find the nearest metastable conformation. After minimization, the temperature was ramped up to between 600 and 900 K at a rate of 0.025 K/iteration. This was then followed by a *NVT* (constant number of particles, constant volume, and constant temperature) equilibration period of 300 000 steps at this temperature (600–900 K) using Berendsen thermostat.⁴² In all cases, a time step of 0.25 fs was used. After the equilibration run, the clusters were annealed to 0 K at a rate of 0.0025 K/iteration. After this, molecular hydrogen was abstracted by removing two hydrogen atoms from the configuration at 0 K. This was done iteratively until all the hydrogen atoms were abstracted. The entire process was repeated several times, each time starting out with $\text{Al}_{28}\text{H}_{84}$ but with a different geometrical arrangement.

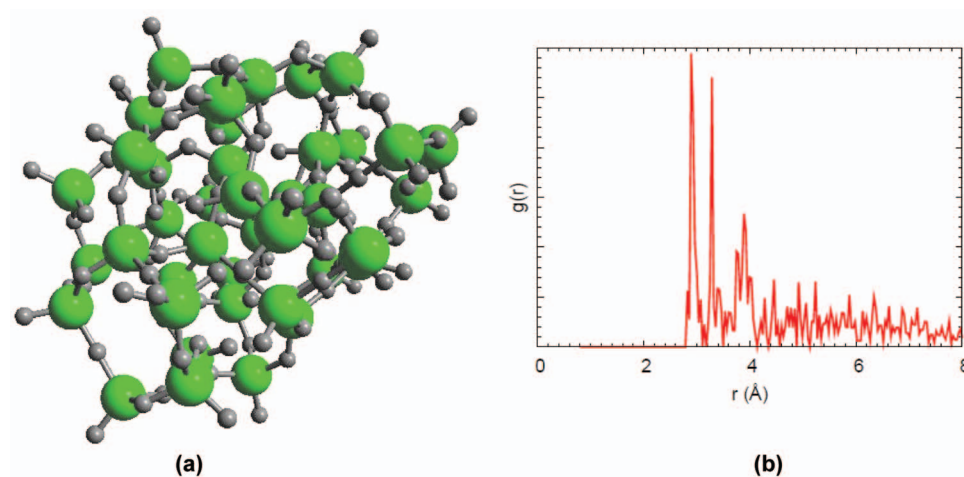
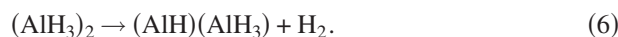


FIG. 8. (a) The completely agglomerated Al_2H_6 clusters at a temperature of 800 K. No molecular hydrogen was desorbed at this temperature. (b) The Al-Al pair distribution function of the cooled agglomerated Al_2H_6 clusters. The agglomerate was annealed to 0 K at a rate of 0.0025 K/iteration.

Only the energies of the most stable conformations that gave rise to the nearly smooth curve shown in Fig. 10 were considered.

Figure 10 shows the trend in particle stability as a function of hydrogen unloading. The negative values of the heat of formation show that at the initial stages the forward decomposition reaction in Eq. (4) is thermodynamically favored. During the abstraction process, the exothermicity of the desorption process decreases with increasing abstraction of molecular hydrogen. When almost a half of the hydrogen atoms have been abstracted, the process becomes endothermic.

The observation can be understood as follows. Region (I) shows the high rate segment when desorption of molecular hydrogen is very favorable, while region (II) is the slow rate segment when desorption of molecular hydrogen systematically becomes unfavorable. The cluster size dependence of the desorption process is related to the local coordination of aluminum atoms with hydrogen. Therefore, the higher the concentration of hydrogen the more favored the decomposition of AlH_3 . Large aluminum clusters can be understood to have a bulklike decomposition as follows:



The reaction in Eq. (6) should be interpreted as follows. The AlH_3 unit from which the hydrogen is abstracted is embedded in other AlH_3 units. There is a saturation of AlH_3 species in the cluster such that each AlH_3 species is surrounded by other AlH_3 species. This provides facile paths for hydrogen desorption as they can make Al–Al metal bonds to compensate for the loss of H–Al bonds. The critical point in Fig. 10 is the point at which there is a transition from exothermicity to endothermicity. In other words, the abstraction of hydrogen starts to become unfavorable since the system is stabilized. We can understand the stable region as follows. There are fewer hydrogen atoms in comparison to aluminum atoms. This implies that the AlH_3 units are dispersed within the system and not embedded in other AlH_3 units. Therefore, the abstraction process essentially behaves like dissociation of AlH_3 , $\text{AlH}_3 \rightarrow \text{AlH} + \text{H}_2$, which is energetically unfavorable.

Intuitively, one is bound to think that as more and more surface hydrogen atoms are abstracted, the remaining hydrogen atoms should become subsurface and be strongly bound to the aluminum atoms (see Ref. 17). However, this is not the case. As more and more surface hydrogen atoms are abstracted the bulk hydrogen atoms come to the surface. In fact, for $\text{Al}_{28}\text{H}_{84}$ the bulk aluminum atoms are octahedrally coordinated to hydrogen atoms (the average bond lengths are $d_{\text{Al-H}} = 1.64 \text{ \AA}$ and $d_{\text{Al-Al}} = 3.342 \text{ \AA}$), while for $\text{Al}_{28}\text{H}_{42}$ the bulk aluminum atoms are tetrahedrally coordinated to hydrogen atoms (average bond lengths are $d_{\text{Al-H}} = 1.65 \text{ \AA}$ and $d_{\text{Al-Al}} = 2.843 \text{ \AA}$). In the case of Al_{28}H_4 the bulk aluminum atoms have no nearest hydrogen neighbors, instead they are icosahedrally coordinated to neighboring aluminum atoms. The average Al–Al bond length in this case is 2.75 \AA . Notice that $d_{\text{Al-H}}$ remains almost constant throughout the abstraction process, whereas $d_{\text{Al-Al}}$ decreases toward the aluminum bulk value. The decrease in $d_{\text{Al-Al}}$ with increasing abstraction of molecular hydrogen implies that there is a transition toward

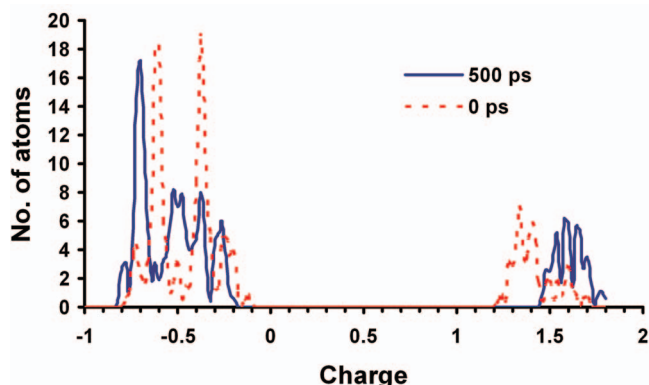


FIG. 9. The charge distribution plots of the alane clusters (0 ps) at the beginning of the simulation and (500 ps) that of the agglomerated cluster at the end of the simulation run.

metallization. On the other hand, the almost constant value of $d_{\text{Al-H}}$ shows that the Al–H bond length is independent of the chemical environment for a given system (in this case binary aluminum hydride). The observations detailed herein show that aluminum atoms prefer to form bond with each other rather than with hydrogen. Hydrogen atoms prefer to stay on the surface rather than subsurface sites and since the surface hydrogen atoms prefer to mostly occupy the less stable twofold (bridge) sites, it becomes easy to desorb them. On the Al(111) surface hydrogen prefers to occupy the three-coordinated hollow (fcc and hcp) sites. The fact that hydrogen atoms prefer to occupy the bridge sites in clusters of this size shows that the surface has a corrugated morphology. The behavior of aluminum hydride cluster is therefore very different from that of NaH .¹⁷ It is also markedly different from that of MgH_2 . Wagemans⁴⁷ showed that the hydrogen atoms in hydrogen depleted magnesium hydride prefer to cluster together instead of being evenly distributed. Using REAXFF, Cheung *et al.*¹⁸ showed that there are no surface hydrogen atoms for hydrogen depleted Mg_{20}H_x ($x=2,4,6$) systems.

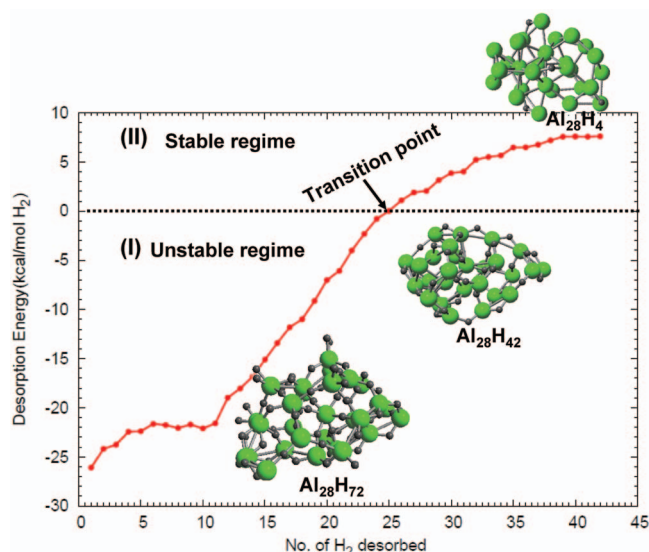


FIG. 10. Desorption energy E^{desorb} as a function of number of H_2 molecules abstracted from the system. The reference energy, shown by the dotted line, is the energy for $\text{Al}_{28}\text{H}_{84}$.

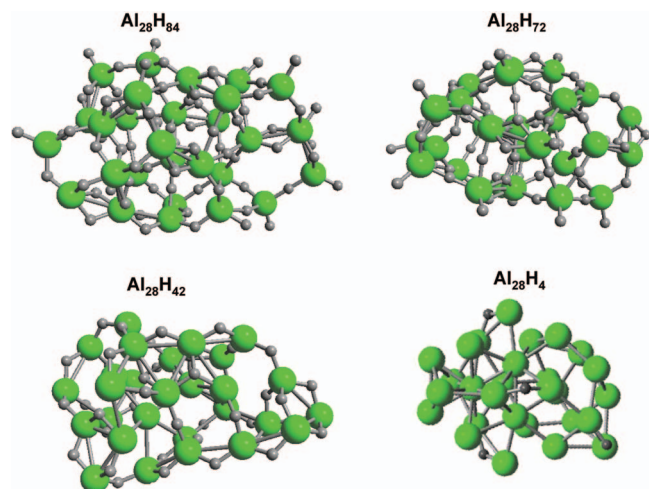


FIG. 11. Geometries of the annealed clusters of $\text{Al}_{28}\text{H}_{84}$, $\text{Al}_{28}\text{H}_{72}$, $\text{Al}_{28}\text{H}_{42}$, and Al_{28}H_4 . In the hydrogen deficient Al_{28}H_4 cluster the hydrogen atoms prefer to occupy surface sites rather than bulk.

We find a different behavior for hydrogen atoms in aluminum hydride systems. In a hydrogen depleted aluminum hydride cluster, the hydrogen atoms are randomly scattered over the aluminum rich surface. This can be seen in Fig. 11, which shows the geometries of the annealed clusters of $\text{Al}_{28}\text{H}_{84}$, $\text{Al}_{28}\text{H}_{72}$, $\text{Al}_{28}\text{H}_{42}$, and Al_{28}H_4 .

The dynamics taking place within the structure during the systematic abstraction of molecular hydrogen can be understood better by examining charge transfer. To investigate the changes in charge transfer due depletion of hydrogen atom, charge distribution plots were made for $\text{Al}_{28}\text{H}_{84}$, $\text{Al}_{28}\text{H}_{42}$, and Al_{28}H_4 clusters during the abstraction runs. This is illustrated in Fig. 12. As shown in Fig. 12, in $\text{Al}_{28}\text{H}_{84}$ there is a broad distribution of charges on both aluminum and hydrogen. This is because there are many subsurface and surface hydrogen atoms. The low charges are associated with surface atoms, which have less number of neighbors. As one moves from $\text{Al}_{28}\text{H}_{84}$ to Al_{28}H_4 the distribution of charges of aluminum atoms tends toward the lower numbers, and concomitantly there is an increase in the negative charge on hydrogen atoms. This is reflected in the charge distribution on $\text{Al}_{28}\text{H}_{42}$ as illustrated in Fig. 12. However, we see in Fig. 12 that the charges located at the hydrogen atoms in Al_{28}H_4 actually decrease. We can understand this disparity as fol-

lows. Since charge distribution is a function of the number of nearest neighbors, this shows that with increasing abstraction of hydrogen there is a decrease in the number of nearest neighbors of opposite charge for both aluminum and hydrogen. The four hydrogen atoms are not subsurface but rather occupy surface sites where they are lowly coordinated to aluminum neighbors. Therefore, they have less number of aluminum atom neighbors. This makes them to have low negative charges. In the case of aluminum, at this point the aluminum atoms have formed metallic bonds since the number of hydrogen in the system is negligible. In other words the system tends toward metallization. In Al_{28}H_4 there are three aluminum atoms that have icosahedral coordination. These aluminum atoms, therefore, have a bulk coordination. This suggests that once almost half the hydrogen atoms have been removed the hydrogen deficient aluminum hydride tends toward metallization.

V. MOLECULAR HYDROGEN TRAPPED IN ALUMINUM HYDRIDE SOLID

For many years now, there have been discussions on the possibility of molecular hydrogen being trapped in the channels of potential hydrogen storage materials such as NaAlH_4 and AlH_3 .^{48–51} The issue of hydrogen molecules being trapped in cages or channels of hydrogen storage media will present the next technological challenges with a view to fully harnessing the storage capabilities of these systems. Trapped molecular hydrogen implies that not all the desorbed hydrogen diffuses out during the thermal decomposition process of the potential hydrogen storage materials. This reduces the efficiency of these materials. How to channel out these trapped hydrogen molecules from the system during the desorption process is clearly a nontrivial task. Using nuclear magnetic resonance (NMR) spectra, Herberg *et al.* deduced that there were molecular hydrogen trapped in small cages in the interstitial sites of NaAlH_4 .⁵² Recent experimental work, using proton NMR, by Senadheera *et al.* showed that molecular hydrogen can be trapped in solid matrix of AlH_3 during the thermal decomposition of AlH_3 .⁵³ To simulate this possibility a cluster of AlH_3 , consisting of 472 atoms, was heated up. The cluster was built up from a supercell of $\beta\text{-AlH}_3$ by removing the periodic boundary conditions. $\beta\text{-AlH}_3$ has very open channels compared to the α -phase.

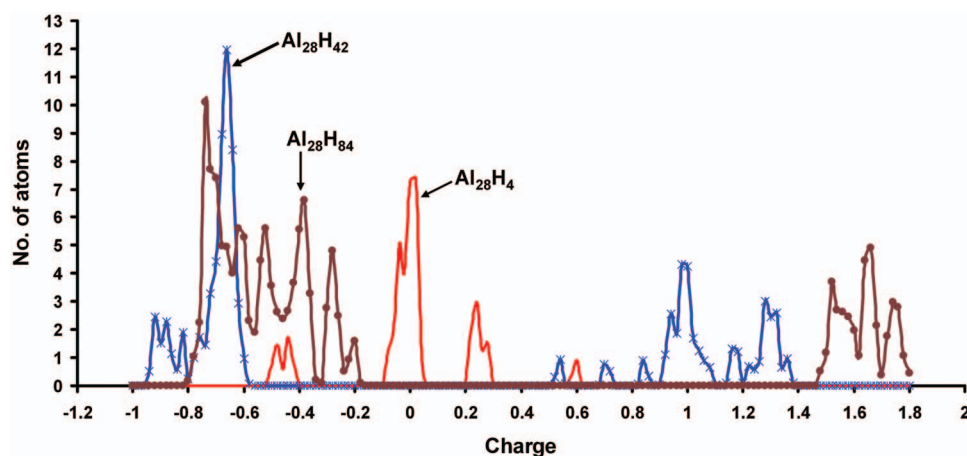


FIG. 12. Charge distribution plots showing the transfer of charge during abstraction process of molecular hydrogen from $\text{Al}_{28}\text{H}_{84}$ cluster. The hydrogen atoms are negatively charged.

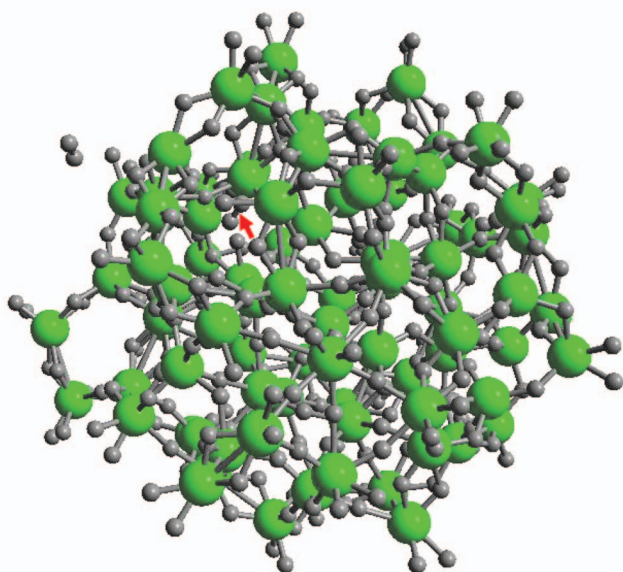


FIG. 13. The arrow shows a hydrogen molecule trapped in AlH_3 channel.

The resultant cluster was first minimized then equilibrated at 300 K. The equilibrated cluster was then heated to 800 K, at a heating rate of 0.0025 K/iteration. This temperature (800 K) was maintained for 120 ps. Figure 13 shows a hydrogen molecule, indicated by an arrow, trapped in the channels of the cluster.

There are dispersive van der Waals interactions between the trapped molecule and the walls of the cages. The trapped molecular hydrogen easily diffuses along the channels into different cages of the cluster. It was noticed that after sometime the molecule escaped. At a faster heating rate the molecular hydrogen escaped at a much earlier time due to the collapse of some cages of the cluster. Even at a constant temperature of 500 K, the molecular hydrogen escaped after sometime although at this temperature it took much longer time to escape.

These results therefore presents an unambiguous identification that molecular hydrogen can be trapped in AlH_3 matrix and for that matter other hydrogen storage materials. We should re-emphasize that our cluster consisted of only 472 atoms (with an approximate width of 1.6 nm). In experiments, usually after ball milling, the size of the particles vary from 150 to 200 nm. Such a particle can contain as much as hundreds of thousands of atoms. This implies that several hundreds or even thousands of molecular hydrogen can be trapped in cages or interstitial sites within such a solid matrix during its thermal decomposition.

VI. CONCLUSION

Based on DFT derived values for bond dissociation profiles, charge distribution, reaction energy data for small clusters, and EoSs for Al and AlH_3 condensed phases, a reactive force field, (REAXFF AlH_3), has been parametrized for AlH_3 systems. REAXFF AlH_3 is built on the same formalism as previous REAXFF descriptions.^{17,18} We find that REAXFF AlH_3 correctly reproduces there DFT data. For the experimentally stable α - AlH_3 phase, REAXFF gives a heat of formation of

-3.1 kcal/mol H_2 , which compares excellently with DFT value of -2.36 kcal/mol H_2 . The experimental heat of formation ranges from -2.37 ± 0.1 kcal/mol H_2 (Ref. 2) to -2.72 ± 0.2 kcal/mol H_2 .⁸

In the gas phase, there is a thermodynamically driven agglomeration of AlH_3 molecules due to the tendency of the system toward attaining a lower free energy configurations. In the initial stages the dominant factor contributing to desorption of hydrogen is the local rise in temperature during the agglomeration process, which weakens/dissociates the Al–H bond. However, as the size of the agglomerated cluster increases the large cluster size effect starts to play a decisive role in desorption of hydrogen. The other contributing factor, to a smaller extent, is the intercluster attraction, which weakens the Al–H bond leading to desorption of molecular hydrogen in a nearby cluster as the clusters move toward each other. The presence of defects such as stepped surfaces accelerates the formation of alane oligomers. These simulation results, especially the oligomerization process, are qualitatively consistent with the experimental work of Go *et al.*,⁵⁴ who noted that heating of alanes at 360 K led to “loss of both mobile and smaller alanes to higher alanes and to desorption.” They showed that small alane clusters do agglomerate to form large clusters but added that experimental limitations might hinder the observation of the resultant compound aluminum hydride clusters.

In the abstraction process of molecular hydrogen, it was seen that with increasing abstraction the remaining hydrogen atoms prefer to occupy surface sites rather than subsurface sites. This behavior is quite different from that of NaH (Ref. 17) and MgH_2 (Refs. 18 and 47) clusters in which with increasing abstraction of molecular hydrogen the remaining hydrogen atoms prefer subsurface sites. In the gas phase, there is a thermodynamically driven agglomeration of alane molecules. In the process of agglomeration, molecular hydrogen is desorbed from the oligomer. Using the method of MD, based on REAXFF, we have unambiguously identified a molecular hydrogen trapped in the AlH_3 matrix.

ACKNOWLEDGMENTS

This work was supported by the Advanced Chemical Technologies for Sustainability (ACTS), which is funded by Nederlandse Organisatie voor Wetenschappelijk Onderzoek (NWO). J.G.O.O. acknowledges fruitful discussions with Jason Graetz and Andreas Zuttel.

- ¹F. M. Brower, N. E. Matzek, P. F. Reigler, H. W. Rinn, C. B. Roberts, D. L. Schmidt, J. A. Snover, and K. Terada, *J. Am. Chem. Soc.* **98**, 2450 (1976).
- ²J. Graetz and J. J. Reilly, *J. Alloys Compd.* **424**, 262 (2006).
- ³J. W. Turley and H. W. Rinn, *Inorg. Chem.* **8**, 18 (1969).
- ⁴X. Ke, A. Kuwabara, and I. Tanaka, *Phys. Rev. B* **71**, 184107 (2005).
- ⁵J. Graetz and J. J. Reilly, *J. Phys. Chem. B* **109**, 22181 (2005).
- ⁶M. Baranowski and B. Tkacz, *Z. Phys. Chem. Neue Folge* **135**, 27 (1983).
- ⁷S. K. Kononov and B. M. Bulychev, *Inorg. Chem.* **34**, 172 (1995).
- ⁸G. C. Sinke, L. C. Walker, F. L. Oetting, and D. R. Stull, *J. Chem. Phys.* **47**, 2759 (1967).
- ⁹B. Bogdanović and G. Sandrock, *MRS Bull.* **27**, 712 (2002).
- ¹⁰G. Sandrock, J. Reilly, J. Graetz, W.-M. Zhou, J. Johnson, and J. Wegrzyn, *Appl. Phys. A: Mater. Sci. Process.* **80**, 687 (2005).
- ¹¹G. Sandrock, J. Reilly, J. Graetz, W.-M. Zhou, J. Johnson, and J.

- Wegrzyn, *J. Alloys Compd.* **421**, 185 (2006).
- ¹² A. Strachan, A. C. van Duin, D. Chakraborty, S. Dasgupta, and W. A. Goddard, *Phys. Rev. Lett.* **91**, 098301 (2003).
- ¹³ A. C. T. van Duin, A. Strachan, S. Stewman, Q. Zhang, X. Xu, and W. Goddard III, *J. Phys. Chem. A* **107**, 3803 (2003).
- ¹⁴ Q. Zhang, T. Qian, A. C. T. van Duin, W. A. Goddard, Y. Qi, and L. G. Hector, *Phys. Rev. B* **69**, 045423 (2004).
- ¹⁵ J. G. O. Ojwang, R. van Santen, G. J. Kramer, A. C. T. van Duin, and W. A. Goddard, *J. Chem. Phys.* **129**, 244506 (2008).
- ¹⁶ A. C. T. van Duin, S. Dasgupta, F. Lorant, and W. Goddard III, *J. Phys. Chem. A* **105**, 9396 (2001).
- ¹⁷ J. G. O. Ojwang, R. van Santen, G. J. Kramer, A. C. T. van Duin, and W. A. Goddard, *J. Chem. Phys.* **128**, 164714 (2008).
- ¹⁸ S. Cheung, W. Deng, A. C. T. van Duin, and W. A. Goddard III, *J. Phys. Chem. A* **109**, 851 (2005).
- ¹⁹ J. K. Gross, S. Guthrie, S. Takara, and G. Thomas, *J. Alloys Compd.* **297**, 270 (2000).
- ²⁰ J. G. O. Ojwang, R. van Santen, G. J. Kramer, and X. Ke, *J. Solid State Chem.* **181**, 3037 (2008).
- ²¹ R. T. Walters and J. H. Scogin, *J. Alloys Compd.* **379**, 135 (2004).
- ²² J. Tersoff, *Phys. Rev. Lett.* **61**, 2879 (1988).
- ²³ D. W. Brenner, *Phys. Rev. B* **42**, 9458 (1990).
- ²⁴ W. J. Mortier, S. K. Ghosh, and S. Shankar, *J. Am. Chem. Soc.* **108**, 4315 (1986).
- ²⁵ G. Kresse and J. Furthmüller, *Phys. Rev. B* **54**, 11169 (1996).
- ²⁶ P. E. Blöchl, *Phys. Rev. B* **50**, 17953 (1994).
- ²⁷ J. P. Perdew, J. A. Chevary, S. H. Vosko, K. A. Jackson, M. R. Pederson, D. J. Singh, and C. Fiolhais, *Phys. Rev. B* **46**, 6671 (1992).
- ²⁸ J. P. Perdew, K. Burke, and Y. Wang, *Phys. Rev. B* **54**, 16533 (1996).
- ²⁹ J. P. Perdew, K. Burke, and M. Ernzerhof, *Phys. Rev. Lett.* **77**, 3865 (1996).
- ³⁰ H. J. Monkhorst and J. D. Pack, *Phys. Rev. B* **13**, 5188 (1976).
- ³¹ R. Dovesi, M. Causà, R. Orlando, C. Roetti, and V. R. Saunders, *J. Chem. Phys.* **92**, 7402 (1990).
- ³² R. Dovesi, V. R. Saunders, C. Roetti, R. Orlando, C. M. Zicovich-Wilson, F. Pascale, B. Civalieri, K. Doll, N. M. Harrison, I. J. Bush *et al.*, *CRYSTAL06 User's Manual* (University of Torino, Torino, 2008).
- ³³ R. Stumpf, *Phys. Rev. Lett.* **78**, 4454 (1997).
- ³⁴ H. Hjelmberg, *Surf. Sci.* **81**, 539 (1979).
- ³⁵ H. Kawamura, V. Kumar, Q. Sun, and K. Yoshiyuki, *Phys. Rev. A* **67**, 063205 (2003).
- ³⁶ C. Wolverton, V. Ozoliņš, and M. Asta, *Phys. Rev. B* **69**, 144109 (2004).
- ³⁷ H. Grove, M. H. Sørby, H. W. Brinks, and B. C. Hauback, *J. Phys. Chem. C* **111**, 16693 (2007).
- ³⁸ J. P. Maehlen, V. A. Yartys, R. V. Denys, M. Fichtner, C. Frommenc, B. M. Bulychiev, P. Pattison, H. Emerich, Y. E. Filinchuk, and D. Chernyshov, *J. Alloys Compd.* **446–447**, 280 (2007).
- ³⁹ G. Henkelman and H. Jónsson, *J. Chem. Phys.* **113**, 9978 (2000).
- ⁴⁰ G. Henkelman, B. P. Uberuaga, and H. Jónsson, *J. Chem. Phys.* **113**, 9901 (2000).
- ⁴¹ X. Tang, B. Laube, D. Anton, S.-J. Hwang, and R. Bowman, APS Meeting Abstracts, 2007 (unpublished), p. 39008.
- ⁴² H. J. C. Berendsen, J. P. M. Postma, W. F. van Gunsteren, A. Dinola, and J. R. Haak, *J. Chem. Phys.* **81**, 3684 (1984).
- ⁴³ K. Lammertsma and J. Leszczyński, *J. Phys. Chem.* **94**, 2806 (1990).
- ⁴⁴ X. Wang, A. Lester, S. Tam, M. E. DeRose, and M. E. Fajardo, *J. Am. Chem. Soc.* **125**, 9218 (2003).
- ⁴⁵ M. Shen and H. F. Schaefer III, *J. Chem. Phys.* **96**, 2868 (1992).
- ⁴⁶ B. K. Rao, P. Jena, S. Burkart, G. Ganteför, and G. Seifert, *Phys. Rev. Lett.* **86**, 692 (2001).
- ⁴⁷ R. W. P. Wagemans, Ph.D. thesis, Universiteit Utrecht, 2006.
- ⁴⁸ G. Majer, E. Stanik, L. E. Valiente Banuet, F. Grinberg, O. Kircher, and M. Fichtner, *J. Alloys Compd.* **404–406**, 738 (2005).
- ⁴⁹ O. J. Zogal, M. Punkkinen, E. E. Ylinen, and B. Stalinski, *J. Phys.: Condens. Matter* **2**, 1941 (1990).
- ⁵⁰ V. P. Tarasov, S. I. Bakum, and S. F. Kuznetsova, *Russ. J. Inorg. Chem.* **42**, 694 (1997).
- ⁵¹ V. P. Tarasov and G. A. Kirakosyan, *Russ. J. Inorg. Chem.* **42**, 1223 (1997).
- ⁵² J. L. Herberg, R. S. Maxwell, and E. H. Majzoub, *J. Alloys Compd.* **417**, 39 (2006).
- ⁵³ L. Senadheera, E. M. Carl, T. M. Ivancic, M. S. Conradi, R. C. Bowman, Jr., S. J. Hwang, and T. J. Udovic, *J. Alloys Compd.* **463**, 1 (2008).
- ⁵⁴ E. Go, K. Thuermer, and J. E. Reutt-Robey, *Surf. Sci.* **437**, 377 (1999).